

Robust thermal boundary conditions applicable to a wall along which temperature varies in lattice-gas cellular automata

Jae Wan Shim*

Nano Science Research Division, Korea Institute of Science and Technology, 136-791 Seoul, Republic of Korea

Renée Gatignol

Institut Jean le Rond d'Alembert, Université Pierre et Marie Curie and CNRS, 4 Place Jussieu, 75252 Paris cedex 05, France

(Received 18 May 2009; revised manuscript received 5 February 2010; published 19 April 2010)

We show that the heat exchange between fluid particles and boundary walls can be achieved by controlling the velocity change rate following the particles' collision with a wall in discrete kinetic theory, such as the lattice-gas cellular automata and the lattice Boltzmann method. We derive a relation between the velocity change rate and temperature so that we can control the velocity change rate according to a given temperature boundary condition. This relation enables us to deal with the thermal boundary whose temperature varies along a wall in contrast to the previous works of the lattice-gas cellular automata. In addition, we present simulation results to compare our method to the existing and give an example in a microchannel with a high temperature gradient boundary condition by the lattice-gas cellular automata.

DOI: [10.1103/PhysRevE.81.046703](https://doi.org/10.1103/PhysRevE.81.046703)

PACS number(s): 47.11.-j, 02.50.Cw, 05.20.Dd

I. INTRODUCTION

In the kinetic theory of gases, the method of discretization of velocities, in which the particle velocities are represented by a given finite set of vectors, was used by Broadwell [1,2], and later by Gatignol [3]. In these works, although the particle velocity was discretized, space and time were continuous. In comparison with their works, Hardy and Pomeau [4] and Hardy *et al.* [5] proposed a square lattice model, the HPP model, which discretizes not only the velocity but also space and time, and studied transport properties of fluids. Frisch *et al.* [6] studied a hexagonal lattice, the FHP model, to avoid the isotropy problem of the square lattice model. The HPP and FHP models are called lattice-gas cellular automata (LGCA), which are arrays of discrete cells with discrete values [7].

The LGCA has the disadvantage of statistical noise as does the Boolean model. However, this problem could be reduced by using single-particle distribution functions, which have real values, instead of Boolean values [8]. We call this method the lattice Boltzmann method (LBM). The LBM with the Bhatnagar-Gross-Krook (BGK) collision term [9], compared to the LGCA, is noise-free, and has Galilean invariance and a velocity independent pressure [10]. As compared with the previous works, which derives the LBM from the LGCA, there are direct derivations of the LBM from the continuous Boltzmann equation [11,12].

For the thermal flows, McNamara and Alder [13] succeeded in simulating the three dimensional heat-transfer problem by using multispeed discrete velocities. In general, there are two major approaches to simulating the thermal

LBM (TLBM): the multispeed approach [13–15], which has problems of numerical instability and limited temperature variation and, the double-population approach [16], which is numerically more stable but still limited in incompressible flows. Recently, Prasianakis and Karlin [17] proposed a thermal LBM based on a so-called consistent LBM [18] and it was demonstrated that the speed of sound and shock propagation are described correctly in a wide temperature range. Nie *et al.* [19] derived a thermal LBM for gases with internal degrees of freedom and showed numerical simulations. However, the simulations were quasi-one-dimensional and did not consider the energy and momentum exchange between wall and flow.

In the early work of the boundary condition in discrete kinetic theory, Gatignol [20] studied gas surface interaction and obtained an H theorem for discrete velocity gases in a vessel. In the early stage of the LGCA simulations, the bounce-back scheme was used for a no-slip boundary condition [6,7]. Later Cornubert *et al.* [21], Ziegler [22], and Ginzbourg and Adler [23] found that this scheme is the first order in numerical accuracy at the boundaries. Ziegler [22] noticed that the imaginary wall between the first row nodes of wall and the first row outside, proposed by Cornubert *et al.* [21], have the second order in numerical accuracy.

There are other boundary schemes proposed to enhance the numerical accuracy of the LBM [24–26]. Zou *et al.* [27] and He *et al.* [28] studied the boundary conditions using the analytical solutions of the LBM. He *et al.* [28] showed that the schemes proposed by Noble *et al.* [25] and Inamuro *et al.* [26] yielded the correct zero-slip velocity, and the bounce-back scheme with the wall located halfway between a flow node and a bounce-back node produced results of second-order accuracy. Ginzburg and d'Humières [29] proposed an approach to deal with inclined flat walls or curved walls. Several authors proposed various boundary conditions based on a link approach [30–32]. Bouzidi *et al.* [31], especially,

*Present address: Interdisciplinary Fusion Technology Division, Korea Institute of Science and Technology. jae-wan.shim@polytechnique.org

proposed a simple way to deal with boundaries of arbitrary geometry in the LBM. They combined the intuitive notion of bounce-back and interpolations. Ginzburg and d'Humières [33] extended the approach of Bouzidi *et al.* [31] to derive boundary conditions for general flows, such that the magnitudes of the Knudsen layers are only third-order corrections to the kinetic problem. Ansumali and Karlin [34] proposed a discrete version of the Maxwell boundary condition, which was earlier postulated by Gatignol [20] in the context of discrete velocity models of the kinetic theory. Guo *et al.* [35] showed that the bounce-back and specular-reflection scheme, and the discrete Maxwell boundary scheme are virtually equivalent, in principle.

For the thermal boundary conditions, many schemes are proposed [16,36–41]. However, it is known that thermal boundary conditions for the TLBM suffer from having negative valued distribution functions, which is a completely unphysical characteristic. Therefore, in the present work, we propose an original boundary condition for the thermal LGCA, which is robust for a high temperature gradient boundary condition. For this purpose, we derive a relation between a temperature and a velocity change rate on a boundary wall, based on Maxwell-Boltzmann statistics, so that we can implant a high gradient temperature boundary condition by adjusting a velocity change rate. Note that this boundary condition can be used for the TLBM when we want to avoid numerical instability caused by the negative values of the distribution function.

II. BOUNDARY CONDITIONS: GENERAL PRESENTATION

A. Lattice gas cellular automata

We define a set of discrete velocities for a two-dimensional model, as an example, by

$$\vec{v}_i = \begin{cases} (0,0) & \text{where } i = 0 \\ c[\cos(i\pi/3), \sin(i\pi/3)] & \text{where } i = 1, 2, 3, 4, 5, 6 \\ 2c[\cos(i\pi/3), \sin(i\pi/3)] & \text{where } i = 7, 8, 9, 10, 11, 12 \end{cases}, \quad (1)$$

where c is a constant. During a fixed discrete time Δt , particles with discrete velocities in formula (1) can move around by hopping from one site to another. We define the discretized space by the sites, i.e., nodes, where particles can exist. The collision process is accompanied after each movement. The rule of collision is that if density, momentum, and energy are the same between two configurations, collision can occur.

B. Thermal lattice Boltzmann method

If we suppose that there is no external force and utilize the BGK collision term [9], the Boltzmann equation is expressed by

$$\begin{aligned} \frac{\partial f(\vec{x}, \vec{v}, t)}{\partial t} + \vec{v} \cdot \vec{\nabla} f(\vec{x}, \vec{v}, t) \\ = - \frac{1}{\tau_{rx}} [f(\vec{x}, \vec{v}, t) - f^{\text{eq}}(\vec{x}, \vec{v}, t)] \end{aligned} \quad (2)$$

where the distribution function f is defined such that $f(\vec{x}, \vec{v}, t)d\vec{x}d\vec{v}$ is the number of particles in an infinitesimal element of phase space $d\vec{x}d\vec{v}$ at time t . The symbol τ_{rx} is a relaxation time that adjusts the attitude to approach the Maxwell-Boltzmann distribution due to collision. The Maxwell-Boltzmann distribution f^{eq} describes the most probable equilibrium state in a given condition. It has a form in two-dimensional space,

$$\begin{aligned} f^{\text{eq}}(\vec{x}, \vec{v}, t) = f^{\text{eq}}(\vec{v}, n, \vec{u}, \tau) \\ = \frac{n}{\pi\tau} \exp\left(-\frac{|\vec{v} - \vec{u}|^2}{\tau}\right) \end{aligned} \quad (3)$$

where τ is defined by $\tau = 2kT/m$, k is the Boltzmann constant, T is a temperature, m is a molecular mass, n is the number density defined by $n = \int f(\vec{x}, \vec{v}, t)d\vec{v}$, and \vec{u} is the macroscopic velocity defined by $\vec{u} = \frac{1}{n} \int \vec{v} f(\vec{x}, \vec{v}, t)d\vec{v}$. If we discretize phase space and time in formula (2), we obtain the TLBM (i.e., Thermal Lattice Boltzmann Method). Initially, we can obtain time discretization in second-order accuracy [42]. In addition, if we define a lattice space and a set of discrete velocities as formula (1), the discretization is complete. The main work of the discretization is that of f^{eq} with respect to \vec{v} . Let f^{eq}_i being a discretized f^{eq} where the subscript i of f^{eq}_i corresponds to the discrete velocity \vec{v}_i .

In two-dimensional space, we can discretize f^{eq} to obtain the TLBM [43] by

$$f^{\text{eq}}_i(\vec{v}_i, \tau) = np_i \{ \psi(\vec{v}_i) + \varphi(\vec{v}_i, \tau) \}, \quad (4)$$

where $\psi(\vec{v}_i) = 1 + 2\vec{v}_i \cdot \vec{u} + 2(\vec{v}_i \cdot \vec{u})^2 - |\vec{u}|^2$,

$$\begin{aligned} \varphi(\vec{v}_i, \tau) = (\tilde{\tau} - 1)(-1 + |\vec{v}_i|^2) + \frac{(\tilde{\tau} - 1)^2}{2}(2 - 4|\vec{v}_i|^2 + |\vec{v}_i|^4) \\ + 2(\tilde{\tau} - 1)(-2 + |\vec{v}_i|^2)(\vec{v}_i \cdot \vec{u}), \end{aligned}$$

with $\vec{v}_i = \vec{v}_i / \sqrt{\tau_0}$, $\vec{u} = \vec{u} / \sqrt{\tau_0}$, $\tilde{\tau} = \tau / \tau_0$, and $\tau_0 = 2kT_0/m$, where T_0 is a reference temperature, and with appropriate p_i of formula (4), which are weight coefficients for discretization of the continuous Maxwell-Boltzmann distribution [11,43]. For example, we have

$$p_i = \begin{cases} 1/4 & \text{where } i = 0 \\ 1/9 & \text{where } i = 1, 2, 3, 4, 5, 6 \\ 1/72 & \text{where } i = 7, 8, 9, 10, 11, 12 \end{cases} \quad (5)$$

for the discrete 13 velocities defined by formula (1) with $c = \sqrt{\tau_0}$.

C. Derivation of a relation between the velocity change rate and temperature

We define discrete velocities of a two-dimensional model in a general form by

$$\vec{v}_i = \begin{cases} c_0[\cos(i\theta_0 + \delta_0), \sin(i\theta_0 + \delta_0)] & \text{where } i = n_{-1} + 1 \text{ to } n_0 \\ c_1[\cos(i\theta_1 + \delta_1), \sin(i\theta_1 + \delta_1)] & \text{where } i = n_0 + 1 \text{ to } n_1 \\ c_k[\cos(i\theta_k + \delta_k), \sin(i\theta_k + \delta_k)] & \text{where } i = n_{k-1} + 1 \text{ to } n_k \\ \dots & \\ c_m[\cos(i\theta_m + \delta_m), \sin(i\theta_m + \delta_m)] & \text{where } i = n_{m-1} + 1 \text{ to } n_m \end{cases}, \quad (6)$$

where $0 \leq c_0 < c_1 < c_2 < \dots < c_m$ and $n_{-1} = -1$. If we consider a homogeneous lattice space, it is natural that we have a property of θ_k which is $(n_k - n_{k-1})\theta_k = 2\pi$ where $k = 1, 2, \dots, m$. If we define $\mathbf{N}_k = n_k - n_{k-1}$ then the previous relation becomes $\mathbf{N}_k \theta_k = 2\pi$.

We define a rate of velocity change $P_{\alpha,\beta}$ from \vec{v}_α to \vec{v}_β as a result of the heat exchange between a site on a boundary and molecules which collide with the site. Note that \vec{v}_α is an initial velocity and \vec{v}_β is a reflected velocity. For example, a site which has $P_{1,2} = 1$ means the velocity change from \vec{v}_1 to \vec{v}_2 occurs 100% for the molecules colliding the site. The rate $P_{k,k}$ means the molecules keep their initial velocity. For a fixed index k of $P_{k,i}$, we have $\sum_{i=0}^{n_m} P_{k,i} = 1$ to conserve the number of molecules.

We recall the thermal accommodation coefficient $\sigma_T = \frac{\tau - \tau_0}{\tau_w - \tau_0}$, which is the measure of efficiency for heat exchange between molecules and a wall, where τ_0 is the temperature before an interaction with the wall, τ is the reflected temperature, and τ_w is the wall temperature. The coefficient $\sigma_T = 1$ signifies that the reflected temperature is equal to the wall temperature.

Definition of hypothesis \mathbf{H}_1 . When the particle colliding with a wall is heated, i.e., the temperature before interaction with the wall τ_0 is lower than the boundary wall temperature τ_w at a position on a wall, we assume that $P_{\alpha,\beta} = 0$ when $|\vec{v}_\alpha| \geq |\vec{v}_\beta|$ and $P_{\alpha,\beta} \geq 0$ when $|\vec{v}_\alpha| < |\vec{v}_\beta|$ for the case of $\alpha \neq \beta$. If $\alpha = \beta$, it is possible that $P_{\alpha,\beta} > 0$ because $P_{k,k}$ indicates the rate of molecules which maintain their initial velocity. Similarly, when the particle colliding with a wall is cooled, i.e., the flow temperature τ_0 is higher than the boundary wall temperature τ_w , we assume that $P_{\alpha,\beta} \geq 0$ when $|\vec{v}_\alpha| > |\vec{v}_\beta|$ and $P_{\alpha,\beta} = 0$ when $|\vec{v}_\alpha| \leq |\vec{v}_\beta|$ for the case of $\alpha \neq \beta$. A temperature gradient can be implanted on a wall by adjusting $P_{\alpha,\beta}$.

We define an index set $\{c_k\}$, utilizing a velocity amplitude c_k in formula (6), by $\{c_k\} = \{n_{k-1} + 1, n_{k-1} + 2, \dots, n_k\}$ where $k = 0, 1, 2, \dots, m$. In other words, $\{c_k\}$ is the set of index numbers i of \vec{v}_i having its amplitude c_k , and there are \mathbf{N}_k different indexes. In addition, an element of $\{c_k\}$ is defined by $\bar{c}_k \in \{c_k\}$, i.e., a certain index in the index set of $\{c_k\}$. We will use this definition, for example, $P_{\alpha,\bar{c}_k} \in [P_{\alpha,i} | i \in \{c_k\}]$.

We recall that the number density f_i is the number of molecules, having the discrete velocity \vec{v}_i , per unit volume. Generally, we can say

$$f_k(\tau, \vec{u}) = \sum_{i=0}^{n_m} P_{i,k} f_i(\tau_0, \vec{u}) \quad \text{where } k = 0, 1, 2, \dots, n_m. \quad (7)$$

Formula (7) shows that the number density at temperature τ , can be described by the number density at temperature τ_0 . At

temperature τ , the molecules having a discrete velocity \vec{v}_k are composed of some of the molecules having a discrete velocity \vec{v}_k at τ_0 , i.e., $P_{k,k} f_k(\tau_0, \vec{u})$ and the molecules initially having discrete velocities \vec{v}_i where $i \neq k$ at τ_0 but becoming \vec{v}_k , i.e., $\sum_{i=0, i \neq k}^{n_m} P_{i,k} f_i(\tau_0, \vec{u})$.

For simplicity, let us consider the case of heating by collision. Therefore, we consider the case of $\tau_w > \tau_0$. With this restriction we apply \mathbf{H}_1 , and then we obtain relations

$$f_{\bar{c}_0}(\tau, \vec{u}) = P_{\bar{c}_0, \bar{c}_0} f_{\bar{c}_0}(\tau_0, \vec{u}), \quad (8)$$

$$f_{\bar{c}_k}(\tau, \vec{u}) = \left(1 - \sum_{i=n_k+1}^{n_m} P_{\bar{c}_k, i} \right) f_{\bar{c}_k}(\tau_0, \vec{u}) + \sum_{i=0}^{n_k-1} P_{i, \bar{c}_k} f_i(\tau_0, \vec{u}), \quad (9)$$

where $k = 1, 2, \dots, m-1$ and

$$f_{\bar{c}_m}(\tau, \vec{u}) = f_{\bar{c}_m}(\tau_0, \vec{u}) + \sum_{i=0}^{n_{m-1}} P_{i, \bar{c}_m} f_i(\tau_0, \vec{u}). \quad (10)$$

It is emphasized that $P_{\alpha,\beta} = 0$ when $|\vec{v}_\alpha| = |\vec{v}_\beta|$ in the case of $\alpha \neq \beta$ (cf. \mathbf{H}_1).

Definition of hypothesis \mathbf{H}_2 . When $\vec{u} \approx 0$;

- (1) $P_{\bar{c}_0, \alpha} = P_{\bar{c}_0, \beta}$ where $\alpha, \beta \in \{c_k\}$ and $k = 1, 2, \dots, m$.
- (2) $P_{\bar{c}_i, \bar{c}_p} = P_{\theta(\bar{c}_i, \bar{c}_p)}$ where $\theta(\bar{c}_i, \bar{c}_p) = \cos^{-1} \left(\frac{|\vec{v}_{\bar{c}_i} \cdot \vec{v}_{\bar{c}_p}|}{|\vec{v}_{\bar{c}_i}| |\vec{v}_{\bar{c}_p}|} \right)$.
- (3) $f_\alpha(\tau, \vec{u}) = f_\beta(\tau, \vec{u})$ where $\alpha, \beta \in \{c_k\}$ and $k = 0, 1, 2, \dots, m$.

We introduced the isotropy of $P_{\alpha,\beta}$ in \mathbf{H}_2 . This enables us to greatly simplify formulas (8)–(10).

We define $P([\bar{c}_l], [\bar{c}_p]) = \sum_{i=n_{p-1}+1}^{n_p} P_{\bar{c}_l, i}$ and $P([\bar{c}_l], \bar{c}_p) = \sum_{i=n_{l-1}+1}^{n_l} P_{i, \bar{c}_p}$. For example, the meaning of $P([\bar{c}_l], [\bar{c}_p])$ is the sum of the velocity change rate $P_{\bar{c}_l, i}$ where $i = n_{p-1} + 1, n_{p-1} + 2, \dots, n_p$, i.e., the index i runs for all \vec{v}_i having an amplitude c_p . Note that $P([\bar{c}_l], [\bar{c}_p]) = P([\bar{c}_l], \bar{c}_p)$ when $\mathbf{N}_l = \mathbf{N}_p$ because $P_{\bar{c}_l, \bar{c}_p}$ does not depend on $\vec{v}_{\bar{c}_l}$ and $\vec{v}_{\bar{c}_p}$ but depends on the angle $\cos^{-1} \left(\frac{|\vec{v}_{\bar{c}_l} \cdot \vec{v}_{\bar{c}_p}|}{|\vec{v}_{\bar{c}_l}| |\vec{v}_{\bar{c}_p}|} \right)$ according to (2) of \mathbf{H}_2 . If we assume $\mathbf{N}_k = \mathbf{N}_s$ where $k, s = 0, 1, 2, \dots, m$, and use \mathbf{H}_2 and $\sum_{i=0}^{n_m} P_{k,i} = 1$, we can rewrite formulas (8)–(10) by

$$f_{\bar{c}_0}(\tau, \vec{u}) = \left(1 - \sum_{p=1}^m P([\bar{c}_0], \bar{c}_p) \right) f_{\bar{c}_0}(\tau_0, \vec{u}), \quad (11)$$

$$f_{\bar{c}_k}(\tau, \vec{u}) = \left(1 - \sum_{p=k+1}^m P([\bar{c}_k], \bar{c}_p) \right) f_{\bar{c}_k}(\tau_0, \vec{u}) + \sum_{l=0}^{k-1} P([\bar{c}_l], \bar{c}_k) f_{\bar{c}_l}(\tau_0, \vec{u}), \quad (12)$$

where $k=1, 2, \dots, m-1$ and

$$f_{\bar{c}_m}(\tau, \vec{u}) = f_{\bar{c}_m}(\tau_0, \vec{u}) + \sum_{l=0}^{m-1} P([\bar{c}_l], \bar{c}_m) f_{\bar{c}_l}(\tau_0, \vec{u}). \quad (13)$$

Note, that for the assumption of $\mathbf{N}_k = \mathbf{N}_s$ where $k, s = 0, 1, 2, \dots, m$, we can have multiple identical velocities with the amplitude of zero, when $c_0=0$, according to the index system of formula (6), for the purpose of using $P(\bar{c}_l, [\bar{c}_p]) = P([\bar{c}_l], \bar{c}_p)$. If we do not use the degeneracy in zero velocity, we have $P(\bar{c}_0, [\bar{c}_p]) \neq P([\bar{c}_0], \bar{c}_p)$ because $P([\bar{c}_0], \bar{c}_p) = P_{\bar{c}_0, \bar{c}_p} = \frac{1}{6} P(\bar{c}_0, [\bar{c}_p])$. In addition, we assume that $P([\bar{c}_0], \bar{c}_p) \geq 0$ when $p \geq 1$.

We define $G_{l,p}$ by the relation $P(\bar{c}_l, [\bar{c}_p]) = G_{l,p} P(\bar{c}_l, [\bar{c}_{l+1}])$ where $G_{l,l+1} = 1$. The physical meaning of $G_{l,p}$ is the ratio between the probability sum of the velocity amplitude change from \bar{c}_l to \bar{c}_p and that from \bar{c}_l to \bar{c}_{l+1} . Formulas (11)–(13) can then be written as

$$f_{\bar{c}_0}(\tau, \vec{u}) = \left(1 - P([\bar{c}_0], \bar{c}_1) \sum_{p=1}^m G_{0,p} \right) f_{\bar{c}_0}(\tau_0, \vec{u}), \quad (14)$$

$$f_{\bar{c}_k}(\tau, \vec{u}) = \left(1 - P(\bar{c}_k, [\bar{c}_{k+1}]) \sum_{p=1}^{m-k} G_{k,k+p} \right) f_{\bar{c}_k}(\tau_0, \vec{u}) + \sum_{l=0}^{k-1} P([\bar{c}_l], \bar{c}_k) f_{\bar{c}_l}(\tau_0, \vec{u}) \quad (15)$$

where $k=1, 2, \dots, m-1$ and

$$f_{\bar{c}_m}(\tau, \vec{u}) = f_{\bar{c}_m}(\tau_0, \vec{u}) + \sum_{l=0}^{m-1} P([\bar{c}_l], \bar{c}_m) f_{\bar{c}_l}(\tau_0, \vec{u}). \quad (16)$$

We introduced $G_{l,p}$ to reduce the number of $P(\bar{c}_l, [\bar{c}_p])$ in formulas (11)–(13). We subsequently calculate $G_{l,p}$, which is first introduced in the literature. This enables us to obtain the thermal boundary condition, which is the relation between temperature and the velocity change rate.

III. APPLICATION TO THE 19-VELOCITIES MODEL

Let us consider a specific case where the discrete velocities are given by

$$\vec{v}_i = \begin{cases} (0, 0) & \text{where } i = 0 \\ c' [\cos(\pi i/3), \sin(\pi i/3)] & \text{where } i = 1, 2, 3, 4, 5, 6 \\ \sqrt{3} c' [\cos(\pi i/3 + \pi/6), \sin(\pi i/3 + \pi/6)] & \text{where } i = 7, 8, 9, 10, 11, 12 \\ 2c' [\cos(\pi i/3), \sin(\pi i/3)] & \text{where } i = 13, 14, 15, 16, 17, 18 \end{cases} \quad (17)$$

Then in formula (6), the constants have values such as $m=3$, $\theta_0 = \theta_1 = \theta_2 = \theta_3 = \pi/3$, $\delta_0 = \delta_1 = \delta_3 = 0$, $\delta_2 = \pi/6$, $c_0 = 0$, $c_1 = c'$, $c_2 = \sqrt{3}c'$, $c_3 = 2c'$, and $\mathbf{N}_0 = \mathbf{N}_1 = \mathbf{N}_2 = \mathbf{N}_3 = 6$. Note that we have six identical velocities having the amplitude of zero, i.e., $\vec{v}_0 = \vec{v}_1 = \vec{v}_2 = \vec{v}_3 = \vec{v}_4 = \vec{v}_5 = 0$ according to the index system of formula (6), for the purpose of using $P(\bar{c}_l, [\bar{c}_p]) = P([\bar{c}_l], \bar{c}_p)$.

Therefore, formulas (14)–(16) become

$$f_{\bar{c}_0}(\tau, \vec{u}) = \{1 - P([\bar{c}_0], \bar{c}_1)(1 + G_{0,2} + G_{0,3})\} f_{\bar{c}_0}(\tau_0, \vec{u}), \quad (18)$$

$$f_{\bar{c}_1}(\tau, \vec{u}) = \{1 - P(\bar{c}_1, [\bar{c}_2]) - G_{1,3} P(\bar{c}_1, [\bar{c}_2])\} f_{\bar{c}_1}(\tau_0, \vec{u}) + P([\bar{c}_0], \bar{c}_1) f_{\bar{c}_0}(\tau_0, \vec{u}), \quad (19)$$

$$f_{\bar{c}_2}(\tau, \vec{u}) = \{1 - P(\bar{c}_2, [\bar{c}_3])\} f_{\bar{c}_2}(\tau_0, \vec{u}) + G_{0,2} P([\bar{c}_0], \bar{c}_1) f_{\bar{c}_0}(\tau_0, \vec{u}) + P([\bar{c}_1], \bar{c}_2) f_{\bar{c}_1}(\tau_0, \vec{u}), \quad (20)$$

and

$$f_{\bar{c}_3}(\tau, \vec{u}) = f_{\bar{c}_3}(\tau_0, \vec{u}) + G_{0,3} P([\bar{c}_0], \bar{c}_1) f_{\bar{c}_0}(\tau_0, \vec{u}) + G_{1,3} P([\bar{c}_1], \bar{c}_2) f_{\bar{c}_1}(\tau_0, \vec{u}) + P([\bar{c}_2], \bar{c}_3) f_{\bar{c}_2}(\tau_0, \vec{u}). \quad (21)$$

If we express $P(\bar{c}_l, [\bar{c}_p])$ by the density distributions, we have, from formula (18),

$$P(\bar{c}_0, [\bar{c}_1]) = \frac{f_{\bar{c}_0}(\tau_0, \vec{u}) - f_{\bar{c}_0}(\tau, \vec{u})}{f_{\bar{c}_0}(\tau_0, \vec{u})(1 + G_{0,2} + G_{0,3})} \quad (22)$$

and, from formulas (18) and (19)

$$P(\bar{c}_1, [\bar{c}_2]) = \frac{1}{f_{\bar{c}_1}(\tau_0, \vec{u})(1 + G_{0,2} + G_{0,3})(1 + G_{1,3})} \times \{ [f_{\bar{c}_1}(\tau_0, \vec{u}) - f_{\bar{c}_1}(\tau, \vec{u})](1 + G_{0,2} + G_{0,3}) + f_{\bar{c}_0}(\tau_0, \vec{u}) - f_{\bar{c}_0}(\tau, \vec{u}) \}. \quad (23)$$

Finally, from formulas (18)–(20),

$$\begin{aligned}
 P(\bar{c}_2, [\bar{c}_3]) &= \frac{1}{f_{\bar{c}_2}(\tau_0, \vec{u})(1 + G_{0,2} + G_{0,3})(1 + G_{1,3})} \\
 &\times \{ [f_{\bar{c}_0}(\tau_0, \vec{u}) - f_{\bar{c}_0}(\tau, \vec{u})](1 + G_{0,2} + G_{0,2}G_{1,3}) \\
 &+ [f_{\bar{c}_1}(\tau_0, \vec{u}) - f_{\bar{c}_1}(\tau, \vec{u})](1 + G_{0,2} + G_{0,3}) \\
 &+ [f_{\bar{c}_2}(\tau_0, \vec{u}) - f_{\bar{c}_2}(\tau, \vec{u})](1 + G_{0,2} + G_{0,3}) \\
 &\times (1 + G_{1,3}) \}. \quad (24)
 \end{aligned}$$

We put formulas (22)–(24) into formula (21), then we obtain

$$\begin{aligned}
 f_{\bar{c}_0}(\tau_0, \vec{u}) + f_{\bar{c}_1}(\tau_0, \vec{u}) + f_{\bar{c}_2}(\tau_0, \vec{u}) + f_{\bar{c}_3}(\tau_0, \vec{u}) \\
 = f_{\bar{c}_0}(\tau, \vec{u}) + f_{\bar{c}_1}(\tau, \vec{u}) + f_{\bar{c}_2}(\tau, \vec{u}) + f_{\bar{c}_3}(\tau, \vec{u}). \quad (25)
 \end{aligned}$$

Formula (25) has a physical meaning. In fact, we recover the conservation of mass between the states of temperatures τ_0 and τ .

According to the solution of the two-dimensional hexagonal 19-velocities model of the TLBM [43], with the assumption of $\vec{u}=\vec{0}$, we substitute $f_{\bar{c}_k}(\tau, \vec{u})$ and $f_{\bar{c}_k}(\tau_0, \vec{u})$ by

$$\begin{aligned}
 f_{\bar{c}_0}(\tau_0, \vec{0}) &= \frac{n}{3}w_0, \\
 f_{\bar{c}_0}(\tau, \vec{0}) &= \frac{nw_0}{3}\{1 - (\tilde{\tau} - 1) + (\tilde{\tau} - 1)^2\}, \\
 f_{\bar{c}_1}(\tau_0, \vec{0}) &= \frac{nw_1}{3}, \\
 f_{\bar{c}_1}(\tau, \vec{0}) &= \frac{nw_1}{3}\left\{1 + (\tilde{\tau} - 1)(-1 + r^2) + \frac{(\tilde{\tau} - 1)^2}{2}(2 - 4r^2 + r^4)\right\},
 \end{aligned}$$

$$f_{\bar{c}_2}(\tau_0, \vec{0}) = \frac{nw_2}{3},$$

$$\begin{aligned}
 f_{\bar{c}_2}(\tau, \vec{0}) &= \frac{nw_2}{3}\left\{1 + (\tilde{\tau} - 1)(-1 + 3r^2) + \frac{(\tilde{\tau} - 1)^2}{2}(2 - 12r^2 + 9r^4)\right\},
 \end{aligned}$$

$$f_{\bar{c}_3}(\tau_0, \vec{0}) = \frac{nw_3}{3},$$

and

$$\begin{aligned}
 f_{\bar{c}_3}(\tau, \vec{0}) &= \frac{nw_3}{3}\left\{1 + (\tilde{\tau} - 1)(-1 + 4r^2) + \frac{(\tilde{\tau} - 1)^2}{2}(2 - 16r^2 + 16r^4)\right\}.
 \end{aligned}$$

The coefficient w_i and r were obtained from the identification between the discrete and the continuous Boltzmann distributions by using the second-order Taylor expansion of the continuous Boltzmann equation and the Laguerre-like quadrature [43]. Their values are given by $w_0=0.164$, $w_1=0.310$, $w_2=0.011$, $w_3=0.015$, and $r=1.115=c'/\sqrt{\tau_0}$. Note that, because of the degeneracy of the zero velocity, the discrete Maxwell-Boltzmann distribution $f^{\text{eq}}_0(\tau, \vec{u})$ has the relation with $f_{\bar{c}_0}(\tau, \vec{u})$ by $f^{\text{eq}}_0(\tau, \vec{u})=6f_{\bar{c}_0}(\tau, \vec{u})$. Of course, these number density functions satisfy formula (25). In addition, formulas (22)–(24) become

$$P(\bar{c}_0, [\bar{c}_1]) = -\frac{2 - 3\tilde{\tau} + \tilde{\tau}^2}{1 + G_{0,2} + G_{0,3}}, \quad (26)$$

$$P(\bar{c}_1, [\bar{c}_2]) = -\frac{(-1 + \tilde{\tau})\{2(-2 + \tilde{\tau})w_0 + (1 + G_{0,2} + G_{0,3})\{r^2(6 - 4\tilde{\tau}) + 2(-2 + \tilde{\tau}) + r^4(-1 + \tilde{\tau})\}w_1\}}{2(1 + G_{0,2} + G_{0,3})(1 + G_{1,3})w_1}, \quad (27)$$

$$\begin{aligned}
 P(\bar{c}_2, [\bar{c}_3]) &= \frac{1}{2(1 + G_{0,2} + G_{0,3})(1 + G_{1,3})w_2} \{-2(1 + G_{0,2} + G_{0,2}G_{1,3})(2 - 3\tilde{\tau} + \tilde{\tau}^2)w_0 + (1 + G_{0,2} + G_{0,3})\{-[r^4(-1 + \tilde{\tau})^2 \\
 &+ 2(2 - 3\tilde{\tau} + \tilde{\tau}^2) - 2r^2(3 - 5\tilde{\tau} + 2\tilde{\tau}^2)]w_1 - (1 + G_{1,3})[9r^4(-1 + \tilde{\tau})^2 + 2(2 - 3\tilde{\tau} + \tilde{\tau}^2) - 6r^2(3 - 5\tilde{\tau} + 2\tilde{\tau}^2)]w_2\}. \quad (28)
 \end{aligned}$$

From this point, we show the method of the $G_{0,2}$ estimation. We recall that the physical meaning of $G_{l,p}$ is the ratio between the probability sum of the velocity amplitude change from \bar{c}_l to \bar{c}_p and that from \bar{c}_l to \bar{c}_{l+1} .

We define $N_{\alpha\beta}$ by the number of particles which change their velocity amplitude from c_α to c_β after collision with

a wall and by analogy $N_{\alpha\delta}$ from c_α to c_δ . When the heat transferred from the wall to the particles is ΔE , the number of possible cases for the combination of $N_{\alpha\beta}$ and $N_{\alpha\delta}$ is $W = \frac{(N_{\alpha\beta} + N_{\alpha\delta})!}{N_{\alpha\beta}!N_{\alpha\delta}!}$ and the transferred heat is $\Delta E = N_{\alpha\beta}\varepsilon_{\alpha\beta} + N_{\alpha\delta}\varepsilon_{\alpha\delta}$ where $\varepsilon_k = \frac{m}{2}c_k^2$, $\varepsilon_{\alpha\beta} = \varepsilon_\beta - \varepsilon_\alpha = \frac{m(c_\beta^2 - c_\alpha^2)}{2}$, and

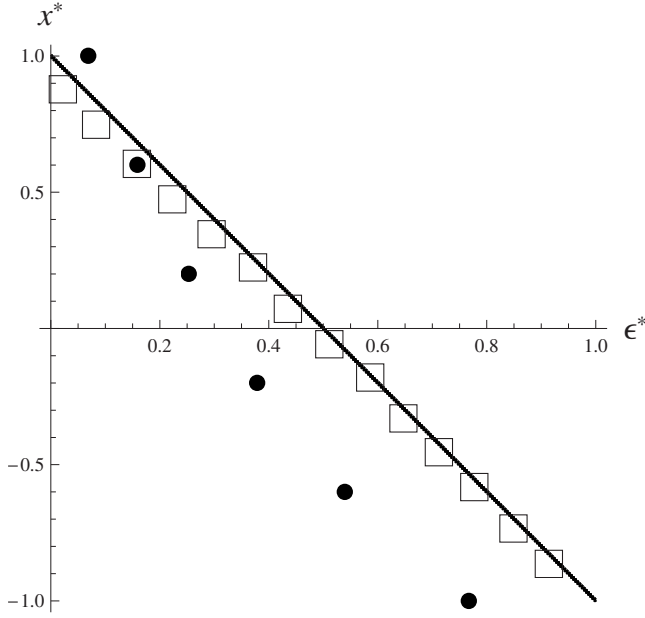


FIG. 1. The comparison of the temperature profile across the channel width. The squares indicate the results of Chen *et al.* [44], the dots indicate our results with $(T_1 - T_0)/T_0 = 0.33$, and the line represents the analytical result.

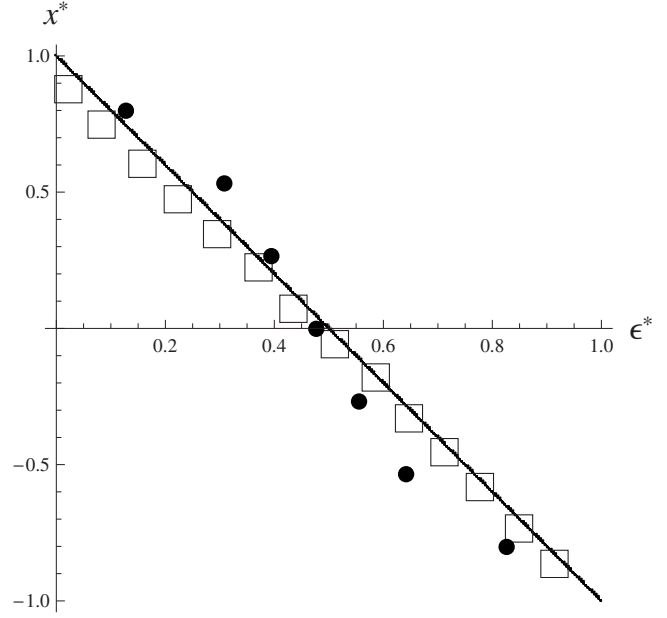


FIG. 2. The comparison of the temperature profile across the channel width. The squares indicate the results of Chen *et al.* [44], the dots indicate our result with $(T_1 - T_0)/T_0 = 0.1$, and the line represents the analytical result.

$\varepsilon_{\alpha\delta} = \varepsilon_\delta - \varepsilon_\alpha = \frac{m(c_\delta^2 - c_\alpha^2)}{2}$. We can calculate the most probable case by virtue of the Lagrange multiplier denoted by χ . We define

$$L = \ln W + \chi(\Delta E - N_{\alpha\beta}\varepsilon_{\alpha\beta} - N_{\alpha\delta}\varepsilon_{\alpha\delta}) \quad (29)$$

then the constraint $\frac{\partial L}{\partial N_{\alpha\beta}} = \frac{\partial L}{\partial N_{\alpha\delta}} = 0$ must be satisfied. We use the Sterling approximation $N! = N^N e^{-N}$. We then obtain

$$\frac{\partial L}{\partial N_{\alpha\beta}} = \ln(N_{\alpha\beta} + N_{\alpha\delta}) - \ln N_{\alpha\beta} - \chi\varepsilon_{\alpha\beta} = 0 \quad (30)$$

and

$$\frac{\partial L}{\partial N_{\alpha\delta}} = \ln(N_{\alpha\beta} + N_{\alpha\delta}) - \ln N_{\alpha\delta} - \chi\varepsilon_{\alpha\delta} = 0. \quad (31)$$

Note that $G_{0,2} = \frac{P([\bar{c}_0], \bar{c}_2)}{P([\bar{c}_0], \bar{c}_1)} = \frac{N_{02}}{N_{01}}$ and $\varepsilon_2 = 3\varepsilon_1$ for the 19-velocities model defined by formula (1). Therefore, when $\alpha=0$, $\beta=1$, and $\delta=2$, formulas (30) and (31) become $\ln(1 + G_{0,2}) = \chi\varepsilon_1$ and $\ln(\frac{1}{G_{0,2}} + 1) = 3\chi\varepsilon_1$, respectively. If we eliminate $\chi\varepsilon_1$ in the last two equations, we obtain

$$\frac{1}{G_{0,2}} + 1 = (1 + G_{0,2})^3. \quad (32)$$

Formula (32) has a positive real valued root $G_{0,2} \approx 0.466$, which is the only positive root.

Similarly, when $\alpha=1$, $\beta=2$, and $\delta=3$, formulas (30) and (31) become $\ln(1 + G_{1,3}) = \chi(\varepsilon_2 - \varepsilon_1) = 2\chi\varepsilon_1$ and $\ln(\frac{1}{G_{1,3}} + 1) = \chi(\varepsilon_3 - \varepsilon_1) = 3\chi\varepsilon_1$, respectively. If we eliminate $\chi\varepsilon_1$ in the last two equations, we obtain

$$\frac{1}{G_{1,3}} + 1 = (1 + G_{1,3})^{3/2}. \quad (33)$$

Formula (33) has a positive real valued root $G_{1,3} \approx 0.755$, which is the only positive root. In addition we have $G_{0,3} \approx 0.380$ from $\frac{1}{G_{0,3}} + 1 = (1 + G_{0,3})^4$, which is obtained the same way as are the calculations of $G_{0,2}$ and $G_{1,3}$. We substitute $G_{0,2}$, $G_{0,3}$, and $G_{1,3}$ in formulas (26)–(28), and use the relation $G_{l,p} = \frac{P(\bar{c}_l, [\bar{c}_p])}{P(\bar{c}_l, [\bar{c}_{l+1}])}$; we then obtain

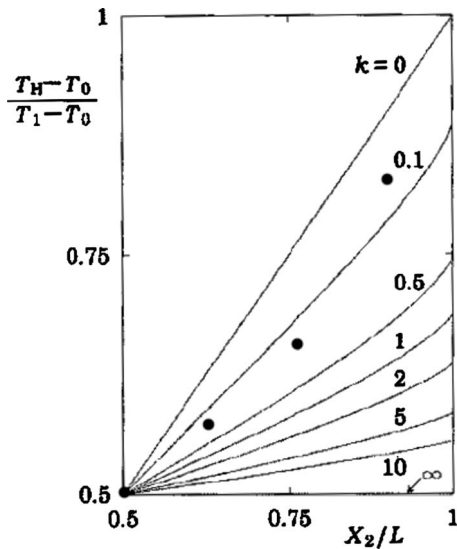


FIG. 3. The comparison of the temperature profile across the channel width. On the figure 4.6 of [45], we added our results by the dots after normalization of temperature.

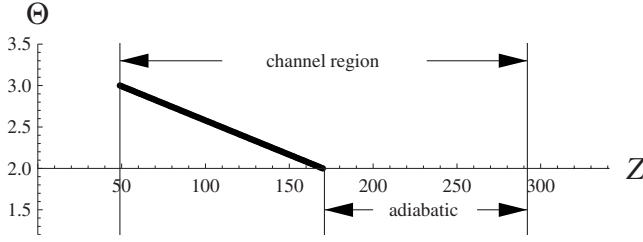


FIG. 4. The thermal boundary condition implanted on the longitudinal wall.

$$\begin{aligned}
 P(\bar{c}_0, [\bar{c}_1]) &= -0.54(2 - 3\bar{\tau} + \bar{\tau}^2), \\
 P(\bar{c}_0, [\bar{c}_2]) &= -0.25(2 - 3\bar{\tau} + \bar{\tau}^2), \\
 P(\bar{c}_0, [\bar{c}_3]) &= -0.21(2 - 3\bar{\tau} + \bar{\tau}^2), \\
 P(\bar{c}_1, [\bar{c}_2]) &= 0.24(-1 + \bar{\tau})(-0.90 + \bar{\tau}), \\
 P(\bar{c}_1, [\bar{c}_3]) &= 0.18(-1 + \bar{\tau})(-0.90 + \bar{\tau}), \\
 P(\bar{c}_2, [\bar{c}_3]) &= 2.60(-1 + \bar{\tau})(-0.33 + \bar{\tau}). \quad (34)
 \end{aligned}$$

We derived the velocity change rate as formula (34) for 19-velocities model. This is for the case of heating by collision as mentioned before. For the case of cooling, the derivation is similar to the case of heating. For example, from formula (22), we obtain $P(\bar{c}_3, [\bar{c}_2]) = \frac{f_{\bar{c}_3}(\tau_0, \bar{u}) - f_{\bar{c}_3}(\tau, \bar{u})}{f_{\bar{c}_3}(\tau_0, \bar{u})(1 + G_{3,1} + G_{3,0})}$. If we write the results, they are

$$\begin{aligned}
 P(\bar{c}_3, [\bar{c}_2]) &= -1.85(-1 + \bar{\tau})(0.16 + \bar{\tau}), \\
 P(\bar{c}_3, [\bar{c}_1]) &= -0.86(-1 + \bar{\tau})(0.16 + \bar{\tau}), \\
 P(\bar{c}_3, [\bar{c}_0]) &= -0.70(-1 + \bar{\tau})(0.16 + \bar{\tau}), \\
 P(\bar{c}_2, [\bar{c}_1]) &= -1.72(-1 + \bar{\tau})(0.875 + \bar{\tau}), \\
 P(\bar{c}_2, [\bar{c}_0]) &= -1.30(-1 + \bar{\tau})(0.875 + \bar{\tau}), \\
 P(\bar{c}_1, [\bar{c}_0]) &= 0.61(-1.665 + \bar{\tau})(-1 + \bar{\tau}). \quad (35)
 \end{aligned}$$

Hence, if $\bar{\tau} \geq 1$, we use formula (34), if $\bar{\tau} < 1$ we use formula (35). Note that formula (35) has all positive values when $\bar{\tau} < 1$; however formula (34) has not when $\bar{\tau} \geq 1$ because of the negative values when $\bar{\tau} > 2$. Therefore, this method is limited to $\bar{\tau} \leq 2$. We use the 19-velocities model for the following simulations. Note that we give the velocity change rate for 13-velocities model in Ref. [43].

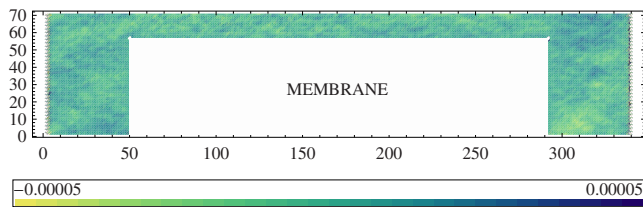


FIG. 5. (Color online) The longitudinal velocity distribution in the microchannel. In the legend, the amplitude of the longitudinal component of \vec{v} is indicated. The node numbers are indicated on the left and the lower sides of the figure.

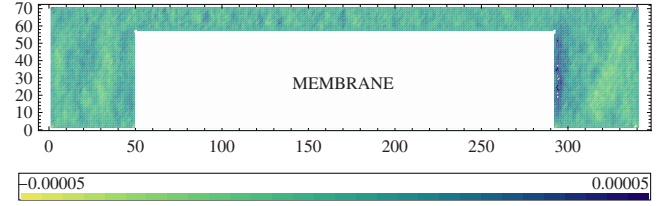


FIG. 6. (Color online) The transversal velocity distribution in the microchannel. In the legend, the amplitude of the transversal component of \vec{v} is indicated. The node numbers are indicated on the left and the lower sides of the figure.

IV. NUMERICAL SIMULATIONS

To apply formula (34) and (35) in the boundary conditions of our simulations, we calculate $\bar{\tau}$ according to the given boundary temperature and the flow temperature. We then obtain $P(\bar{c}_l, [\bar{c}_p])$ at a specific site. Next, for a particle having c_l in this site, we generate a random number between 0 and 1. If this number is equal or less than $P(\bar{c}_l, [\bar{c}_p])$, the velocity amplitude changes from c_l to c_p . However, if this number is more than $P(\bar{c}_l, [\bar{c}_p])$, there is no velocity amplitude change. Note that the discrete velocities having amplitude c_p are multiple. Therefore, the discrete velocity is selected at random.

We compared the results of our method with that of Chen *et al.* [44] who did a simulation of the thermal flow with the LGCA when the thermal boundary temperature was constant along a wall. Note that our method can deal with the thermal boundary whose temperature varies along a wall as well as that whose temperature is constant along a wall. We show these simulations after this comparison.

We compare their results with ours in Figs. 1 and 2. The simulations deal with a flow in a channel between two parallel plates with different temperatures, which is the same problem as that of Chen *et al.* [44]. The inlet and the outlet of the channel generate identical configurations of nodes; therefore, the net flow in the longitudinal direction is zero. In Fig. 1, the given temperatures of the lower and the upper walls are 2.66 and 2.0, respectively. Therefore, we have a temperature difference which is $(T_1 - T_0)/T_0 = 0.33$ where T_1 and T_0 are the high and the low temperatures of the walls. Our simulation occupies 64×66 lattice sites and we use a 10×11 site average to obtain a temperature profile after 10 000 iterations of time average while Chen *et al.* [44] used 512×256 lattice sites and used a large site average. The Knudsen number of our simulation could be calculated by $\text{Kn} \approx \frac{1}{64 \cos(\pi/6)} \approx 0.018$ according to the lattice geometry, which is four times bigger than $\text{Kn} \approx \frac{1}{254 \cos(\pi/6)} \approx 0.004$ of

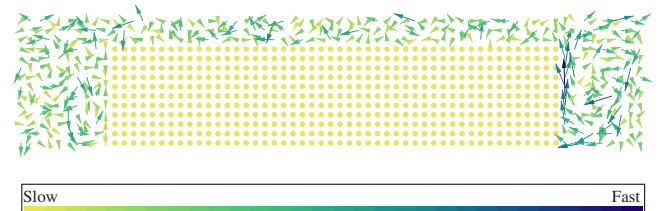


FIG. 7. (Color online) The velocity field distribution in the microchannel.

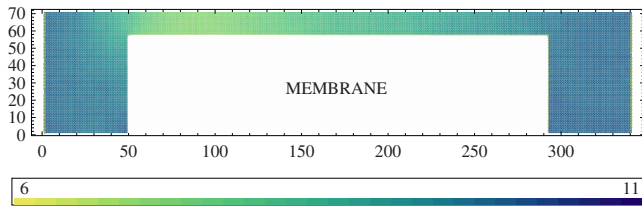


FIG. 8. (Color online) The density distribution in the microchannel. In the legend, the value of N is indicated. The node numbers are indicated on the left and the lower sides of the figure.

Chen *et al.* [44]. Note that the Knudsen number of our simulation $Kn \approx 0.018$ is calculated by the lattice geometry. However, if we consider the fact that the collision does not occur when the configuration of a node has no possible configuration to change, the effective Knudsen number in our simulation could be bigger than $Kn \approx 0.018$ because the mean free path in this case is bigger than the distance between two nodes. The normalization is carried out by $\varepsilon^* = \frac{\varepsilon - \varepsilon_0}{\varepsilon_1 - \varepsilon_0}$ and $x^* = \frac{x}{h}$ where ε_0 and ε_1 are the lowest and the highest temperatures, respectively, and $2h$ is the channel width. We used a conventional PC for the simulation. Therefore, we had difficulty increasing the lattice sites as 512×256 because of the PC's resource power. The analytical result is obtained under the continuum hypothesis. Therefore, our simulation result which is not aligned and has temperature jumps near wall may show the rarefaction effect with the non negligible Knudsen number.

Sone [45] has studied the heat-transfer between two plane walls in a linear case where the temperature differences are small, and has underlined the jumps on the walls and the non linear profile for the temperature. Note that, in contrast to Sone's work, we have, in Fig. 1, a big temperature difference which is $(T_1 - T_0)/T_0 = 0.33$. The temperature jump at $x^* = -1$ is bigger than the jump at $x^* = 1$. The temperature jump is probably more important at the higher temperature wall.

In order to compare better our simulation results with those of Sone [45], we select a small temperature difference between the two walls. Our simulation deals with a flow in a channel between two parallel plates with different temperatures of 2.2 and 2.0 for the lower and the upper plates, respectively. We obtained a temperature profile for $(T_1 - T_0)/T_0 = 0.1$ and $Kn \approx \frac{1}{14 \cos(\pi/6)} \approx 0.082$ according to the lattice geometry. The simulation occupies 64×14 lattice sites and we obtain a temperature profile after 64×2 lattice sites average and time average of 1 000 iterations. The effec-

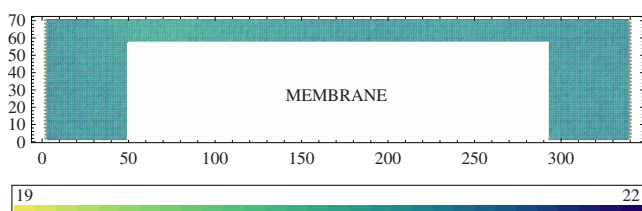


FIG. 9. (Color online) The pressure distribution in the microchannel. In the legend, the value of p^* is indicated. The node numbers are indicated on the left and the lower sides of the figure.

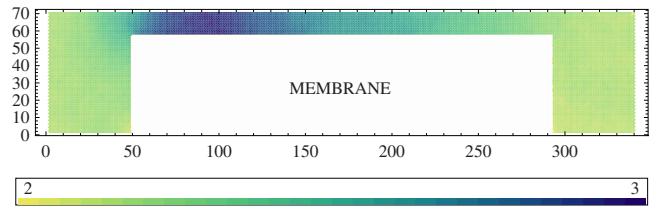


FIG. 10. (Color online) The temperature distribution in the microchannel. In the legend, the value of Θ is indicated. The node numbers are indicated on the left and the lower sides of the figure.

tive Knudsen number in our simulation could be bigger than $Kn \approx 0.082$ because the mean free path in this case is bigger than the distance between two nodes. We present this second simulation result in Fig. 2, on which the results of Chen *et al.* are also indicated.

The comparison between the temperature profile obtained in the second simulation (Fig. 2) and the figure 4.6 of [45] is shown in Fig. 3. The temperature profile obtained by our simulation is not too far from the profile of $Kn=0.1$ of the figure 4.6 of [45].

Henceforth, we show simulation results of the 19-velocities model of the LGCA using the thermal boundary conditions of formulas (34) and (35) in a microchannel, with $1 \mu\text{m}$ width and $10 \mu\text{m}$ length, connected with two chambers of $2 \mu\text{m}$ length. Previously, simulation results have been presented in the same microchannel but for an isothermal problem [46,47]. However, we simulate thermal flows having complicated thermal boundary conditions at this time. Figure 4, which is only the half image with respect to the transversal direction, shows the geometry of the calculation domain which is composed of 341×71 nodes. The Knudsen number is about 0.08.

We present two simulations according to the given boundary conditions. The initial condition of the calculation sites is that the particles having \vec{v}_i where $i = \{1, 4, 7, 10, 13, 16\}$ are occupied and the remainder of the particles are vacant for all sites of the calculation domain. The initial wall boundary condition is same as the thermal boundary condition used during the calculation, which means we use a steady state thermal boundary condition. The entrance and the exit boundary conditions are such that the particles hav-

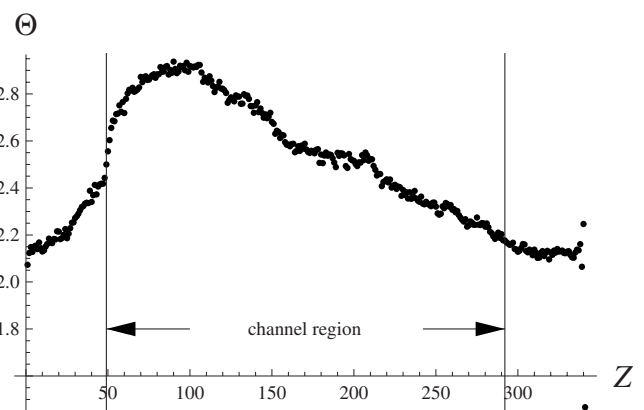


FIG. 11. The value of Θ near the central longitudinal axis in the microchannel.

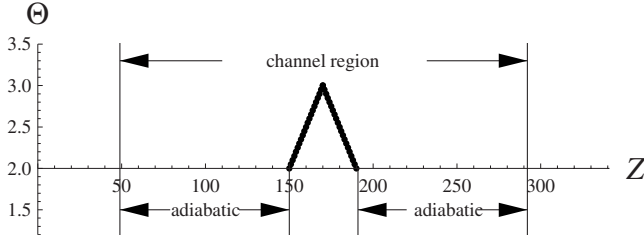


FIG. 12. The thermal boundary condition implanted on the longitudinal wall.

ing \vec{v}_i , where $i=\{3, 6, 9, 12, 13, 15, 16, 18\}$, are generated and the rest of the particles are not for all time t.

The first thermal boundary condition implanted on the longitudinal wall is described in Fig. 4. The left half of the channel region has a high gradient temperature boundary condition and the right half has an adiabatic boundary condition. Note that the flow with the same values of pressure, density, and velocity is generated at the left and right extremities of the left and right chambers (cf. Fig. 5), respectively. We used the thermal accommodation coefficient $\sigma_T=1$. We verified the convergence of the simulated flows by comparing the values with respect to the numbers of iterations.

The longitudinal and the transversal velocity (amplitudes of the longitudinal and transversal components of \vec{v} , respectively) distributions in the microchannel are shown in Figs. 5 and 6. Their values are very small. (Note that $|\vec{v}|=1$ signify $|\vec{v}|=\sqrt{\tau_0}$.) The velocity field distribution is shown in Fig. 7. We observed a vortex in the exit chamber.

Figures 8–10 show the density, pressure, and temperature distributions, respectively. The value of the density is obtained by $N=\sum_{k=0}^{18} N_k$ where $N_k=0$ if \vec{v}_k is not occupied and $N_k=1$ if \vec{v}_k is occupied. The value of the pressure is obtained by $p^*=\sum_{k=0}^{18} N_k (\frac{\vec{v}_k-\vec{u}}{c_1})^2$ where $\vec{u}=\sum_{k=0}^{18} \frac{N_k \vec{v}_k}{N}$. We can obtain the value of the temperature by $\Theta=p^*/N$. The distribution of Θ is that of a scaled temperature because, from the ideal gas kinetic theory, we have $p=nkT$ where p is a pressure, n is a number density, k is the Boltzmann constant, and T is a temperature. Hence, in three-dimensional space we have a relation $\Theta=\frac{m\tau}{2\varpi}$ where m is a molecular mass, ϖ is a volume containing the number of molecules N , and $\tau=\frac{2kT}{m}$. The density and the temperature distributions show inhomogeneity, while the pressure distribution shows homogeneity in the domain of the calculation.

The values of Θ with respect to the longitudinal number of nodes Z near the central longitudinal axis in the micro-

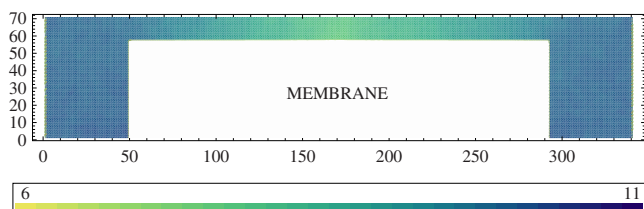


FIG. 13. (Color online) The density distribution in the microchannel. In the legend, the value of N is indicated. The node numbers are indicated on the left and the lower sides of the figure.

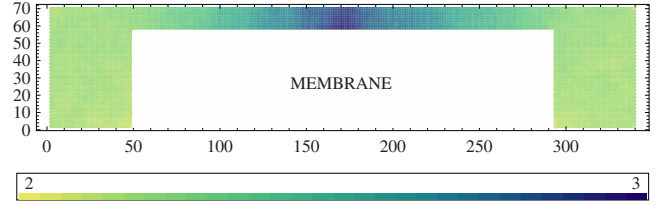


FIG. 14. (Color online) The temperature distribution in the microchannel. In the legend, the value of Θ is indicated. The node numbers are indicated on the left and the lower sides of the figure.

channel are shown in Fig. 11. The results show that the maximum temperature of the flow is located around $Z=100$ although the given temperature boundary condition has a maximum temperature around $Z=50$. In addition, the flow is heated in the entire microchannel and even chambers. The calculation time is less than one day by a conventional PC.

The second thermal boundary condition implanted on the longitudinal wall is described in Fig. 12. The central part of the channel region has a high gradient temperature boundary condition and its left and right sides have the adiabatic boundary conditions. Note that the flow with the same values of pressure, density, and velocity with $\Theta \approx 2$ is generated at the left and right extremities of the left and right chambers (c.f. Fig. 13), respectively. We use the thermal accommodation coefficient $\sigma_T=1$ as before. We obtained the velocity and pressure distributions; however, they were similar to those of the first simulation. Therefore, we omitted them. Figure 13 corresponds to Figs. 8, and Figs. 14 and 15 correspond to Figs. 10 and 11, with respect to their given boundary conditions. The results show that the maximum temperature of the flow is located around $Z=170$ where the given temperature boundary condition has the maximum value. In addition, the flow is heated in the entire microchannel and even chambers.

V. CONCLUSION

The LBM is a promising scheme for simulating isothermal flows in applications involving interfacial dynamics and complex boundaries. For thermal flows, the TLBM was developed, and showed successful simulation results in certain

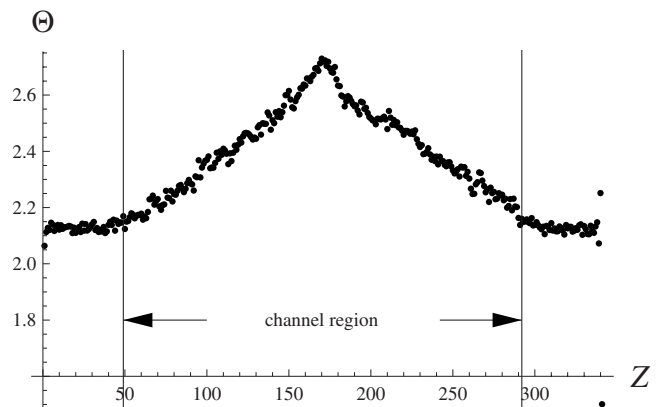


FIG. 15. The value of Θ near the central longitudinal axis in the microchannel.

conditions. However, it is still suffering from the negativity of the discrete distribution functions on the boundary after collision. For thermal flows, we can also use the multispeed LGCA with an original robust thermal boundary condition, which is first suggested in this paper, by introducing $G_{l,p}$ and using Maxwell-Boltzmann statistics. We derived a relation between a temperature and a velocity change rate. Therefore, it was possible to make the effect of heat exchange on a wall, along which we could vary temperature, by adjusting the rate of velocity change. This is a remarkable achievement because, to the best of our knowledge, previous works could only deal with walls having constant temperatures along them in LGCA. We applied our method to the

two-dimensional hexagonal 19-velocities model and derived formulas (34) and (35), and with these results we presented simple thermal flows to compare our method with others and show microchannel flow simulations with high temperature gradient boundary conditions for the LGCA.

ACKNOWLEDGMENTS

J.W.S. is grateful to the Korea Institute of Science and Technology, the Ministry of Education, Science and Technology, and the Ministry of National Defense for the support of his research.

-
- [1] J. E. Broadwell, *Phys. Fluids* **7**, 1243 (1964).
 [2] J. E. Broadwell, *J. Fluid Mech.* **19**, 401 (1964).
 [3] R. Gatignol, *Phys. Fluids* **18**, 153 (1975).
 [4] J. Hardy and Y. Pomeau, *J. Math. Phys.* **13**, 1042 (1972).
 [5] J. Hardy, O. de Pazzis, and Y. Pomeau, *Phys. Rev. A* **13**, 1949 (1976).
 [6] U. Frisch, B. Hasslacher, and Y. Pomeau, *Phys. Rev. Lett.* **56**, 1505 (1986).
 [7] S. Wolfram, *J. Stat. Phys.* **45**, 471 (1986).
 [8] G. R. McNamara and G. Zanetti, *Phys. Rev. Lett.* **61**, 2332 (1988).
 [9] P. L. Bhatnagar, E. P. Gross, and M. Krook, *Phys. Rev.* **94**, 511 (1954).
 [10] Y. H. Qian, D. d’Humières, and P. Lallemand, *EPL* **17**, 479 (1992).
 [11] X. He and L. Luo, *Phys. Rev. E* **55**, R6333 (1997).
 [12] X. Shan, X.-F. Yuan, and H. Chen, *J. Fluid Mech.* **550**, 413 (2006).
 [13] G. McNamara and B. Alder, *Physica A* **194**, 218 (1993).
 [14] F. J. Alexander, S. Chen, and J. D. Sterling, *Phys. Rev. E* **47**, R2249 (1993).
 [15] Y. Chen, H. Ohashi, and M. Akiyama, *Phys. Rev. E* **50**, 2776 (1994).
 [16] X. He, S. Chen, and G. D. Doolen, *J. Comput. Phys.* **146**, 282 (1998).
 [17] N. I. Prasianakis and I. V. Karlin, *Phys. Rev. E* **78**, 016704 (2008).
 [18] S. Ansumali and I. V. Karlin, *Phys. Rev. Lett.* **95**, 260605 (2005).
 [19] X. Nie, X. Shan and H. Chen, *Phys. Rev. E* **77**, 035701(R) (2008).
 [20] R. Gatignol, *Phys. Fluids* **20**, 2022 (1977).
 [21] R. Cornubert, D. d’Humières, and D. Levermore, *Physica D* **47**, 241 (1991).
 [22] D. P. Ziegler, *J. Stat. Phys.* **71**, 1171 (1993).
 [23] I. Ginzbourg and P. M. Adler, *J. Phys. II* **4**, 191 (1994).
 [24] P. A. Skordos, *Phys. Rev. E* **48**, 4823 (1993).
 [25] D. R. Noble, S. Chen, J. G. Georgiadis, and R. O. Buckius, *Phys. Fluids* **7**, 203 (1995).
 [26] T. Inamuro, M. Yoshino, and F. Ogino, *Phys. Fluids* **7**, 2928 (1995).
 [27] Q. Zou, S. Hou, and G. D. Doolen, *J. Stat. Phys.* **81**, 319 (1995).
 [28] X. He, Q. Zou, L.-S. Luo, and M. Dembo, *J. Stat. Phys.* **87**, 115 (1997).
 [29] I. Ginzbourg and D. d’Humières, *J. Stat. Phys.* **84**, 927 (1996).
 [30] O. Filippova and D. Hänel, *Int. J. Mod. Phys. C* **9**, 1271 (1998).
 [31] M. Bouzidi, M. Firdaouss, and P. Lallemand, *Phys. Fluids* **13**, 3452 (2001).
 [32] D. Yu, R. Mei, L.-S. Luo, and W. Shyy, *Prog. Aerosp. Sci.* **39**, 329 (2003).
 [33] I. Ginzburg and D. d’Humières, *Phys. Rev. E* **68**, 066614 (2003).
 [34] S. Ansumali and I. V. Karlin, *Phys. Rev. E* **66**, 026311 (2002).
 [35] Z. L. Guo, B. C. Shi, T. S. Zhao, and C. G. Zheng, *Phys. Rev. E* **76**, 056704 (2007).
 [36] A. D’Orazio and S. Succi, *FGCS, Future Gener. Comput. Syst.* **20**, 935 (2004).
 [37] G. H. Tang, W. Q. Tao, and Y. L. He, *Phys. Rev. E* **72**, 016703 (2005).
 [38] V. Sofonea and R. F. Sekerka, *Phys. Rev. E* **71**, 066709 (2005).
 [39] C. Shu, X. D. Niu, and Y. T. Chew, *J. Stat. Phys.* **121**, 239 (2005).
 [40] Y.-H. Zhang, X. J. Gu, R. W. Barber, and D. R. Emerson, *EPL* **77**, 30003 (2007).
 [41] L. Zheng, Z. L. Guo, and B. C. Shi, *EPL* **82**, 44002 (2008).
 [42] S. Chen and G. D. Doolen, *Annu. Rev. Fluid Mech.* **30**, 329 (1998).
 [43] J. W. Shim, Ph.D. thesis, Université Pierre et Marie Curie (Paris VI), 2008.
 [44] S. Chen, H. Chen, G. D. Doolen, S. Gutman, and M. Lee, *J. Stat. Phys.* **62**, 1121 (1991).
 [45] Y. Sone, *Molecular Gas Dynamics: Theory, Techniques and Application* (Birkhäuser, Boston, 2007), pp. 169–177.
 [46] J. W. Shim and R. Gatignol, *Houille Blanche* **5**, 120 (2009).
 [47] J. W. Shim and R. Gatignol, in *Microchannel Flow With Lattice Gas Cellular Automata and Lattice Boltzmann Method*, AIP Conf. Proc. No. 1084, edited by T. Abe (AIP, New York, 2009), p. 1033.